Molecular simulation of benzene adsorption in graphitic and amorphous carbon slit pores

Ella V. Ivanova,[†] Alina Emelianova,[†] Alexei F. Khalizov,[‡,†] and Gennady Y. Gor[*,†]

[†]*Otto H. York Department of Chemical and Materials Engineering, New Jersey Institute of Technology, University Heights, Newark, NJ 07102, USA*

[‡]*Department of Chemistry and Environmental Science New Jersey Institute of Technology, University Heights, Newark, NJ07102, USA*

E-mail: gor@njit.edu

Abstract

Atmospheric soot consists of fractal aggregates of spherical particles, which are made of ordered (graphitic) and disordered (amorphous) carbon. Condensation of polycyclic aromatic hydrocarbons (PAHs) on the surface of spherical particles and in the junctions between these particles induces morphological changes in soot aggregates. We studied the interactions of benzene molecules with graphitic and amorphous carbon slit pores, where benzene represented PAHs and slit pores represented the junctions between carbon spheres in a soot aggregate. We used Monte Carlo simulations in the grand canonical ensemble (GCMC) to calculate benzene adsorption isotherms and molecular dynamics simulations to analyze benzene fluid structure inside the pores. As expected, graphitic and amorphous carbon confinement results in significantly different adsorption isotherms and the local structure of benzene in the pores. We also found that using two different force fields for benzene (all-atom OPLS and a nine site united

atom TraPPE, which takes into account the quadrupole moment of benzene) produces similar adsorption isotherms, but different orientation of benzene molecules in the pores.

Introduction

Black carbon, the main component of combustion soot, is a major air pollutant and a potent warming agent. It is released by many sources, including internal combustion engines, industrial power plants, biomass burning, and residential heating. After entering the atmosphere, black carbon profoundly affects Earth climate, human health, and many ecosystems despite its relatively low mass concentration in the air.[1,2] Black carbon is not only a pollutant, but also a high-tonnage product manufactured industrially on a large scale for a variety of applications. Commonly known as carbon black, this product, due to its high porosity and high internal surface area, is a common adsorbent for removing various chemicals from gases and liquids.

Although a useful property for the industrial carbon black, the high adsorption capacity of combustion soot in the atmosphere is highly disadvantageous, as it exacerbates its negative environmental impacts. For instance, the surface of soot particles supports the adsorption of higher molecular weight polycyclic aromatic hydrocarbons (PAHs), turning these particles into PAH carriers. The presence of PAHs generated in flames on the particle surface allows to learn more about soot formation mechanisms,[3] but also such particles can deliver toxic PAHs into the human respiratory system. Exposure to PAHs carries an increased health risk due to their carcinogenicity and mutagenicity.[2,4] The exposure can be exacerbated when adsorbed PAHs induce the collapse of fractal aggregates into compact globules (see Fig. 1a).[5] Compaction can bring the particles into the size range that allows them to penetrate deep into the lungs and deposit thereby diffusion with high-efficiency.[6]

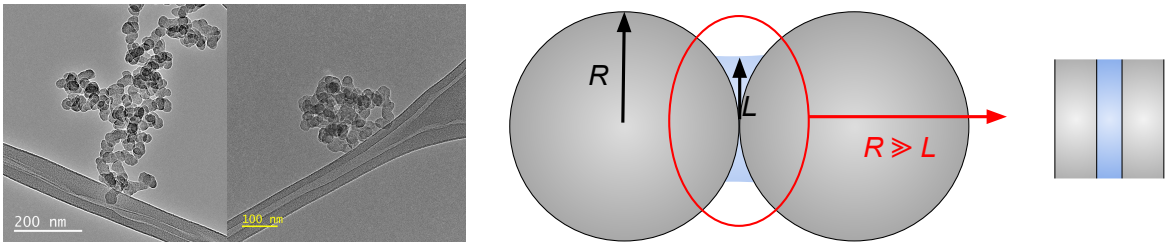

(a) (b)

FIGURE 1: (a) TEM images of soot aggregates: fractal (left) and partially restructured (right). (b) The schematic representation of two carbon monomers in a soot aggregate. Condensate between the monomers drives the aggregate restructuring. For estimating the solvation forces, this system can be further simplified as a slit pore if the radius of the monomers R is much greater than the character size of the liquid bridge L.

The restructuring of fractal soot particles caused by the adsorbate or condensate formed during the interaction with various gaseous chemicals and condensable vapors (such as PAHs) has been a subject of many studies.[5,7–14] It was shown that in certain cases, even a small amount of condensate (e.g., PAH), insufficient to cover the aggregate with a single molecular layer, could cause restructuring.[5,7,8] This phenomenon was rationalized by invoking capillary condensation that placed vapor molecules selectively in the junctions between spherical carbon monomers comprising the fractal soot aggregates.[7] The menisci of condensate in the junctions are thought to be primarily responsible for the capillary and solvation forces leading to the rearrangement of monomers within the soot aggregate and leading to compaction.[7,12] To predict the rate of soot restructuring, it is necessary to evaluate these forces, which depend on both the distribution of the condensate in the junctions and the surface structure of soot monomers. A simple system that can be used for evaluating interfacial properties of soot monomers coated with condensate is a slit pore filled with fluid. The slit pore is a limiting case of two monomers with a meniscus of condensate, provided that the monomers have a radius much larger than the radius of the meniscus (see Fig. 1b).

Soot monomers have a complex internal structure consisting of both amorphous and graphitic carbons, where an amorphous carbon core is surrounded by multiple layers of

crystalline graphite plates arranged in an onion-like manner.[15–17] It has been shown that the monomer structure needs to be reproduced rather closely in order to make accurate predictions of certain properties, e.g., the degree of order of carbon in the inner region of soot monomers may significantly affect their optics.[18] Molecular adsorption on amorphous and graphitic carbon surfaces is also expected to be significantly different because amorphous carbon is composed of sp^2-hybridized carbon atoms arranged in a highly disordered manner, whereas graphite has a highly ordered structure consisting of multiple graphene layers.

There have been a large number of experimental adsorption studies in the form of adsorption isotherm measurement for benzene on different types of carbons,[19–23] but these studies provided only limited structural information about the fluid and it had to be indirectly inferred. In some experimental studies, such as in neutron diffraction work, the structural properties of adsorbed fluid could be directly determined. For instance, Mehan et al.[24] have shown that at lower temperatures benzene molecules aggregate in two-dimensional clusters rather than spreading uniformly over the surface.

Most detailed information about the structure of adsorbed fluid can be obtained using molecular simulations. Many molecular simulation studies were focused on investigating benzene adsorbed on a carbon surface[25–28] or in a slit pore.[29–34] Most studies dealt with graphitic carbon and only a few considered disordered carbon, showing that for certain fluid properties the difference between the two forms of carbon could be significant.[32,34] Fomin compared the behavior of benzene inside amorphous and graphitic carbon slit pores[32] and based on the fluid density profile and orientation of benzene molecules within the fluid showed a significant difference in benzene distribution between the two pore materials. Many studies have reported that molecules of benzene formed a layered structure near the surface.[32–35] Also, within those layers, molecules showed a predominant orientation, preferring to be arranged parallel to the carbon surface. The molecules' orientation results from the interplay between two types of non-covalent interactions: van der Waals and electrostatic interactions.[36] To understand the driving force leading to different orientations, we need to consider the charge

distribution inside benzene molecules. The net dipole moment of benzene is zero because of its symmetry: the six local dipole moments corresponding to six C−H bonds in a benzene molecule cancel each other. However, the benzene molecule has a strong quadrupole moment resulting from the non-uniform charge distribution in a π bonding system represented by a positively charged σ-bond framework and two negatively charged π electron clouds (Fig. 2). The two preferential orientations in benzene fluid with aromatic rings either perpendicular or parallel to each other (see Fig. 3) are a result of the electrostatic π-π and π-σ interactions and van der Waals interactions. Similar interactions need to be considered to determine the preferential orientation of benzene molecules in adsorbate and condensate layers. For instance, Coasne and co-authors have shown that accurate modeling of the interaction between benzene and a polar surface of hydroxylated silica requires a force field that takes into account the quadrupole moment of benzene.[37–39] However, it is not obvious whether there is need to account for the quadrupole moment when modeling benzene interaction with non-polar surfaces, such as carbon.

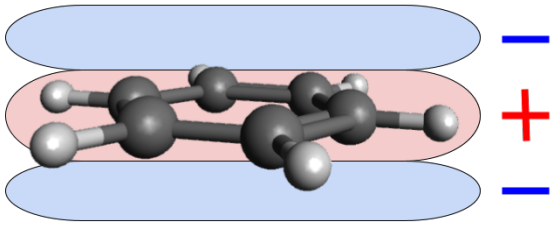

FIGURE 2: The quadrupole charge distribution of benzene

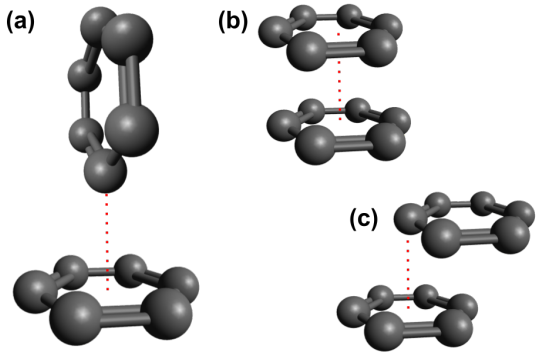

FIGURE 3: π-π interactions between aromatic systems:(a) edge-to-face, (b) sandwich, (c) displaced

Many modeling studies have investigated layering within the fluid, but only a few made a connection between the fluid structure and adsorption isotherms. In this work, we compare the interaction of carbon surfaces made of atomistically ordered (graphitic) and disordered (amorphous) structures with benzene molecules. The latter is used as a surrogate for PAHs, which are commonly present in atmospheric aerosols and can induce soot restructuring. We

used Monte Carlo simulations in the grand canonical ensemble (GCMC) to calculate benzene adsorption isotherms and molecular dynamics simulations to analyze fluid structure inside the pore. Also, using two different force fields for benzene we evaluated how accounting for its quadrupole moment affects the benzene-wall interaction. With these results, we assess the applicability of different soot monomer structures for future modeling the soot restructuring process.

Models and Computational Methods

We consider a carbon slit pore with benzene, comparing two distinct structures of the pore walls: graphitic and amorphous carbon (see Fig. 4). First, we quantify the solid-fluid interaction based on the adsorption isotherm analysis. Second, we investigate how different types of carbon surfaces affect the distribution of benzene molecules.

We used the same geometrical parameters as in the recent research.[32–34] The internal sizes of the pore were the same. The dimensions of the walls were 6.7 Å × 48 Å × 48 Å and the distance between the plates was varied between 10 Å and 20 Å. The number of carbon atoms was 3256 and 5760 for amorphous and graphitic structures, respectively. We studied a fluid distribution in completely-filled pores at a pressure of 10^6 Pa (for amorphous pores of 18 Å and above the pressure was 10^7 Pa).

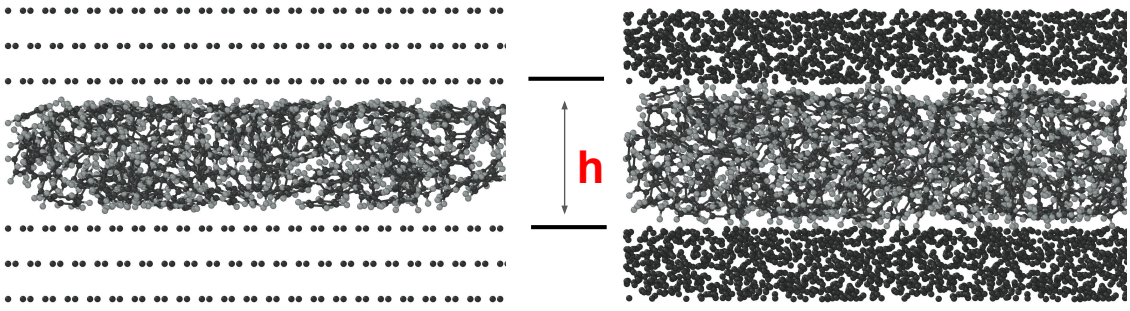

FIGURE 4: Slit carbon pores filled with benzene: pore with graphitic walls (left), pore with amorphous carbon walls (right). The distance between the walls h is the same for both pores. Snapshots were taken for the initial configuration before the simulation run.

The graphitic wall contained 3 graphite layers with the distance between them 3.354 Å[40] (See Figure 4). We used common lattice parameters for graphite: $a = 2.46$ Å and 1.42 Å.[41] Also, the second layer was displaced relative to the outer layers by a distance of 1.42 Å along the axes forming the plane of the graphite layer. Thus, if the second layer is projected onto the first, each hexagon of the first layer will have a carbon atom of the second layer in the center, corresponding to ABA (or Bernal) stacking.

Generating an amorphous carbon structure is more laborious and can be done using several methods.[42–49] In this work, the liquid quench method was used that mimics the actual process of the formation of disordered carbon in a flame.[49] The procedure is described in detail below.

Force Fields

In this work, we considered two force fields for benzene molecules: an all atom model OPLS[50] (Fig. 5a) and a united atom model TraPPE[51] (Fig. 5b), both of which have been widely used for molecular simulation of benzene adsorption.[52–55] The parameters for both force fields are presented in Table 1.

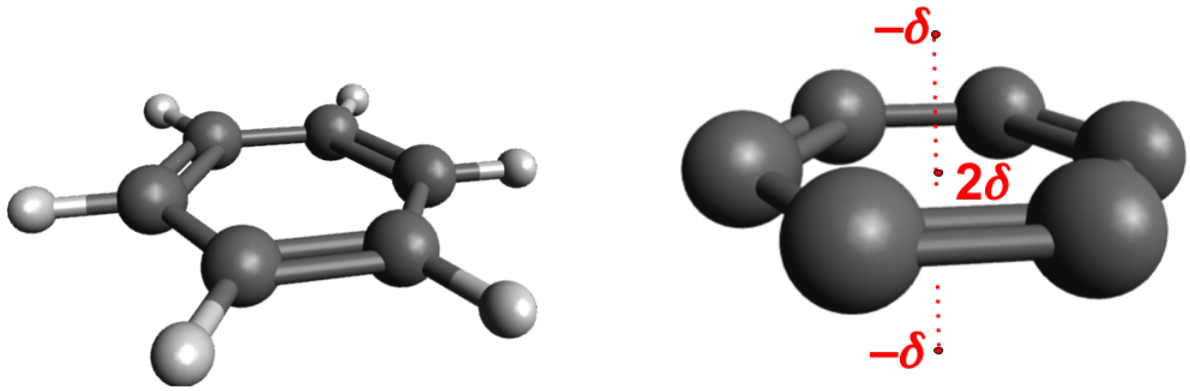

(a) (b)

FIGURE 5: Two representations of a benzene molecule used in this work: an all-atom model used in OPLS (a) and a 9-site united atom model used in TraPPE (b). Parameter δ represents the value of the imaginary charge.

In the OPLS model, each atom had a non-zero partial charge. In contrast, in the TraPPE model, CH group was neutral, but to take into account the quadrupole moment of benzene, three extra/imaginary charges $\{-\delta, -\delta, 2\delta\}$ were included (see Fig. 5b). The first imaginary charge, $I_1 = 2\delta$, was placed in the center of the aromatic ring, the others were located at the distances of $\pm 0.0785\,\text{nm}$ from the center along the axis normal to the plane of the molecule. All bonds and angles were considered rigid for both benzene models.

TABLE 1: Parameters for the OPLS (all atom)[50] and TraPPE (united atom)[51] model of benzene

OPLS							
	r_{CC}	r_{CH}	σ_C	ε_C/k_B	σ_H	ε_H/k_B	q_C	q_H
	1.40 Å	1.08 Å	3.55 Å	35.23 K	2.42 Å	15.097 K	$-0.115\,e$	$0.115\,e$
TraPPE							
	r_{CH-CH}	σ_{CH}	ε_{CH}/k_B	q_{CH}	q_{I_1}	q_{I_2}	q_{I_3}	
	1.40 Å	3.74 Å	48.0 K	$0.0\,e$	$2.42\,e$	$-1.21\,e$	$-1.21\,e$	

To generate the amorphous carbon structure we used bond order potentials introduced by Tersoff .[56] This potential helps to correctly describe chemical reactions, in contrast to the traditional molecular mechanics force field. The LJ parameters for carbon atoms in the walls were 28.0 K and 3.4 Å. Carbon atoms in the slit pore carried a zero partial charge. Also, we used Lennard-Jones potential to describe benzene-graphite interaction. This approach was successfully tested by Vernov and Steele.[25,26] The cross parameters were obtained using the Lorentz-Berthelot mixing rules: $\varepsilon_{12} = \sqrt{\varepsilon_1 \varepsilon_2}$ and $\sigma_{12} = (\sigma_1 + \sigma_2)/2$. The cutoff distance where interactions were truncated is $r_{cut} = 14\,\text{Å}$ and no tail corrections were applied. For calculating electrostatic interactions in periodic molecular systems we used the particle-particle particle-mesh (PPPM).

Generating the amorphous structure of carbon

There are several main techniques to generate the atomic structure of amorphous carbon (see SI). In this work, we used the liquid quench method based on molecular dynamics

simulations[57–61] . The distinctive feature of this method is that it mimics the actual process of the formation of disordered carbon in a flame. Similar to combustion, the amorphous carbon goes from a high-temperature liquid-like state to a low-temperature solid during the simulation.

The modeling steps for the liquid quenching method are based on Ref. 49. The first step in simulation is to create a box containing N (in Ref. 49 $N = 1200$) carbon atoms, which form a simple cubic lattice structure. The initial temperature is set at 10 000 K. The next step is to equilibrate the system. Under these conditions, disordered carbon is formed. The third step is to quench the carbon-box to 3000 K. It should then be annealed at 3000 K and quenched again to 300 K. The last step is equilibration at 300 K. The model mimics the experiment: the high-temperature stage corresponds to the gas phase. The following quench and anneal stages help the formation of disordered carbon at a low temperature.

The quench rate, annealing time, and system size are critical as they affect the final structure of the amorphous carbon (See Ref. 49). The quenching rate affects the hybridization of carbon, where the sp^2 fraction at the end depends on the rate: with decreasing quenching rate, the percent of the sp^2 increases (for more detail see Ref. 49). However, increasing the annealing time leads to getting a well-ordered structure. Thus, it was shown that it is possible to get amorphous carbon with the same density, but with a different internal structure, only by changing the quenching rate or annealing time (see Ref. 49). In this work, we have created amorphous carbon by liquid quenching with parameters given in Table 2. The final amorphous carbon structure was verified based on the density and radial distribution function through comparison with the data from Ref. 62.

Construction and characterization of the slit carbon pore

We created two different carbon wall structures: graphitic and amorphous. The next step was to create a slit pore with a given internal size. It was assumed that the internal size of the pore is equal to the minimal distance between the centers of carbon atoms belonging to

TABLE 2: The parameters of the molecular dynamics simulation for generating the amorphous carbon. The time step is 0.07 ps

process	time
Equilibration at 10^5K	15 ps
Quench to 3×10^3 K	630 ps
Anneal at 3×10^3 K	336 ps
Quench to 3×10^2 K	7 ps
Equilibrate at 3×10^2 K	10 ps

the opposite walls. In contrast to the graphitic wall, the amorphous wall has a rough surface. Since the result of the adsorption is sensitive to the small volume change, the helium void fraction for each of the pores was calculated as implemented in RASPA to estimate the actual available adsorption volume and actual size of the two different carbon pores. The results presented in Table 3 show that there is no significant difference between the nominal and actual pore size. The input files for generating an amorphous structure can be found in Supporting Information.

TABLE 3: Comparison of the pore size: nominal and actual, based on helium void fraction[a]

nominal size	actual size	
	amorphous carbon	graphitic carbon
10 Å	9.56 ± 0.38 Å	9.36 ± 0.54 Å
12 Å	11.76 ± 0.16 Å	11.24 ± 0.32 Å
14 Å	13.52 ± 0.20 Å	13.57 ± 0.74 Å
16 Å	15.75 ± 0.18 Å	15.26 ± 0.62 Å
18 Å	17.62 ± 0.24 Å	17.60 ± 0.38 Å
20 Å	19.50 ± 0.18 Å	19.40 ± 0.74 Å

[a] The uncertainties were estimated from the fluctuations of the ensemble average over the simulation run as two standard deviations.

Grand Canonical Monte Carlo Simulations

The adsorption of benzene in a slit pore was simulated using the grand canonical Monte Carlo (GCMC),[63] which is widely utilized for this purpose. We performed simulations at a

temperature of 298.15 K in the pressure range of 10^{-3} Pa – 10^{6} Pa. The carbon atoms in the pore walls were kept at the initial positions. We found that 10^5 cycles were sufficient for the equilibration period based on the preliminary runs. We used at least 10^5 cycles for the production run, where the number of steps in each cycle equals the maximum between 20 and N, where N is the number of molecules in the system. With equal probability, we considered the following types of moves: displacement, rotation, reinsertion, and deletion. The average properties and configurations of the system were stored every 1000 cycles. The adsorption isotherms were obtained in terms of the number of adsorbed molecules N as a function of pressure P. The pressure was given as an input and related to the chemical potential μ through the Peng–Robinson equation of state[64] as implemented in RASPA,[53] since this is widely used in molecular simulation of benzene adsorption.[54,55] Note, however, that the quality of the PR EOS predictions at high pressures can be low, therefore we also reported the values of chemical potential $\mu = \mu^{\mathrm{ig}} + \mu^{\mathrm{ex}}$, where the excess chemical potential is calculated from the PR EOS, and $\mu^{\mathrm{ig}} = RT \ln (P\Lambda^3/kT)$, Λ is the de Broglie thermal length (see Tables 4-7). For both, amorphous and graphitic nanopores, we used periodic boundary conditions along the directions parallel to the pore surface. Thus, the slit pore corresponded to an infinitely long pore in x and y directions. The uncertainties were calculated according to the procedure implemented in RASPA code.[53] The simulation is divided into 5 blocks, and the standard deviation is calculated. The uncertainty is taken as the 95% confidence interval.

Molecular Dynamics Simulations

In order to analyze the liquid configurations in a slit pore we performed MD simulations in the canonical ensemble. The temperature was kept constant at 298.15 K using a Nose-Hoover thermostat and a barostat with default damping time 0.15 ps. The carbon atoms in the pore walls were fixed at the initial positions during all simulations run. First, we minimized and equilibrated the slit pores for 0.5 ns. Then, statistics were gathered from production periods

of 2 ns. The equations of motion were integrated with a time step of 0.1 fs using the Verlet algorithm.[65]

SOFTWARE. The graphitic wall was constructed using VMD,[66] Packmol[67] and Moltemplate[68,69] software. The simulations were performed in LAMMPS/20200602[70] and RASPA 2.0.35.[53]

Results

Adsorption Isotherms

We obtained benzene adsorption isotherms using two different models. The adsorption isotherm for the OPLS benzene model is shown in Fig. 6a and Tables 4, 5. The isotherm for the TraPPE benzene model is presented in Fig. 6b and Tables 6, 7. Adsorbed amounts N are normalized by N_0, the number of molecules adsorbed at the highest pressure considered, $P = 10^7$ Pa for graphitic and amorphous pores.

Note that we consider only the adsorption branches of the isotherms, because the experimental adsorption isotherms of benzene vapor on microporous carbons are often reversible or show very small hysteresis loops[71–74] of Type H4, according to the the IUPAC classification.[75] It is unlikely that desorption isotherms obtained by GCMC could reproduce the experimental hysteresis loops. Since we considered two different benzene models, we checked the bulk liquid density for both, which showed a good agreement with previously published data.[50,52]

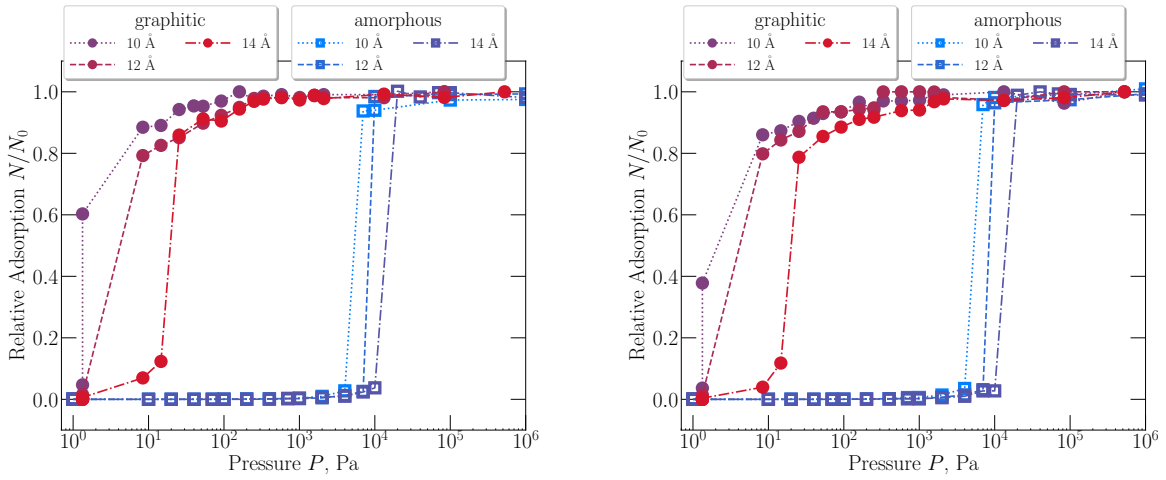

FIGURE 6: Adsorption of benzene for the all atom OPLS (a) and the 9-site united atom TraPPE (b) benzene models in a slit carbon pore at 298.15 K. Amorphous and graphitic structures were used for the carbon walls. Isotherms are based on the adsorption-branch calculations only. The uncertainties were calculated based on 95% confidence intervals

TABLE 4: Adsorption isotherms for all-atom benzene model with OPLS force field. The number of molecules, N, in a slit amorphous carbon pore as a function of pressure at 298.15 K. Isotherms are based on the adsorption-branch calculations only. The uncertainties were calculated based on 95% confidence intervals

P, Pa	μ, kJ/mol	10 Å	12 Å	14 Å	16 Å	18 Å	20 Å
		Amount adsorbed, N					
1	−71.00	0.0 ± 0.0	0.0 ± 0.0	0.0 ± 0.0	0.0 ± 0.0	0.0 ± 0.0	0.0 ± 0.0
10	−65.30	0.0 ± 0.0	0.0 ± 0.0	0.0 ± 0.0	0.0 ± 0.0	0.0 ± 0.0	0.0 ± 0.0
1×10^2	−59.59	0.1 ± 0.0	0.1 ± 0.0	0.1 ± 0.0	0.1 ± 0.0	0.1 ± 0.0	0.1 ± 0.0
2×10^2	−57.87	0.1 ± 0.0	0.1 ± 0.0	0.1 ± 0.0	0.1 ± 0.0	0.1 ± 0.0	0.1 ± 0.0
4×10^2	−56.15	0.3 ± 0.0	0.2 ± 0.0	0.2 ± 0.0	0.2 ± 0.0	0.2 ± 0.0	0.2 ± 0.0
7×10^2	−54.76	0.5 ± 0.0	0.4 ± 0.0	0.4 ± 0.0	0.4 ± 0.0	0.4 ± 0.0	0.4 ± 0.0
1×10^3	−53.88	0.7 ± 0.0	0.6 ± 0.0	0.6 ± 0.0	0.5 ± 0.0	0.5 ± 0.0	0.5 ± 0.0
2×10^3	−52.16	1.5 ± 0.0	1.1 ± 0.0	1.1 ± 0.0	1.1 ± 0.0	1.1 ± 0.0	1.1 ± 0.0
4×10^3	−50.45	3.8 ± 0.2	2.4 ± 0.1	2.3 ± 0.0	2.2 ± 0.0	2.2 ± 0.0	2.2 ± 0.0
7×10^3	−49.06	145.1 ± 2.1	4.9 ± 0.3	4.4 ± 0.1	4.1 ± 0.1	4.1 ± 0.1	4.1 ± 0.1
1×10^4	−48.18	145.8 ± 3.0	177.2 ± 3.7	7.0 ± 0.3	6.2 ± 0.3	6.3 ± 0.1	6.2 ± 0.1
1×10^5	−47.41	148.9 ± 3.8	178.7 ± 2.8	222.0 ± 3.8	9.6 ± 0.7	9.5 ± 0.2	9.5 ± 0.2
1×10^6	−47.33	149.0 ± 3.1	180.0 ± 2.1	219.6 ± 3.4	10.1 ± 0.5	9.8 ± 0.1	9.9 ± 0.6
1×10^7	−46.55	151.0 ± 3.5	181.4 ± 3.4	219.9 ± 1.6	253.5 ± 2.0	24.2 ± 31.2	16.4 ± 0.8

TABLE 5: Adsorption isotherms for all-atom benzene model with OPLS force field. The number of molecules, N, in a slit graphitic carbon pore as a function of pressure at 298.15 K. Isotherms are based on the adsorption-branch calculations only. The uncertainties were calculated based on 95% confidence intervals

P, Pa	μ, kJ/mol	10 Å	12 Å	14 Å	16 Å	18 Å	20 Å
		Amount adsorbed, N					
1	−71.00	0.0 ± 0.0	0.0 ± 0.0	0.0 ± 0.0	0.0 ± 0.0	0.0 ± 0.0	0.0 ± 0.0
10	−65.30	97.7 ± 3.7	116.1 ± 0.9	11.6 ± 0.6	4.7 ± 0.2	7.8 ± 0.3	3.9 ± 0.2
1×10^2	−59.59	104.2 ± 2.4	134.0 ± 2.7	155.8 ± 3.2	48.2 ± 2.9	37.8 ± 0.3	29.5 ± 0.8
2×10^2	−57.87	105.6 ± 1.0	135.6 ± 0.4	159.9 ± 1.5	181.3 ± 2.2	63.5 ± 1.0	53.2 ± 1.2
4×10^2	−56.15	108.7 ± 1.0	139.8 ± 1.2	161.1 ± 2.5	190.9 ± 2.4	221.7 ± 2.2	91.0 ± 0.9
7×10^2	−54.76	106.0 ± 0.4	138.7 ± 5.8	167.2 ± 3.2	195.6 ± 0.9	224.8 ± 1.8	114.8 ± 1.4
1×10^3	−53.88	106.2 ± 1.8	143.9 ± 0.3	164.9 ± 1.3	198.2 ± 3.1	229.3 ± 0.7	249.5 ± 1.7
2×10^3	−52.16	107.2 ± 1.0	143.0 ± 2.7	171.2 ± 2.4	204.8 ± 4.8	232.5 ± 2.7	257.1 ± 2.0
4×10^3	−50.45	105.1 ± 2.6	142.0 ± 2.8	171.1 ± 0.6	206.9 ± 2.3	235.9 ± 1.9	264.4 ± 1.9
7×10^3	−49.06	104.6 ± 1.5	141.0 ± 1.4	172.7 ± 1.6	210.2 ± 2.7	241.7 ± 3.0	269.7 ± 2.8
1×10^4	−48.18	107.1 ± 2.0	144.0 ± 0.1	172.9 ± 2.3	213.0 ± 1.3	242.1 ± 0.9	272.7 ± 1.8
1×10^5	−47.41	107.4 ± 0.9	144.0 ± 0.0	174.3 ± 1.4	213.5 ± 1.6	243.0 ± 1.1	274.1 ± 2.2
1×10^6	−47.33	108.5 ± 0.9	146.7 ± 0.5	174.7 ± 0.8	214.7 ± 2.3	243.6 ± 3.6	273.6 ± 1.8
1×10^7	−46.55	108.0 ± 1.3	149.5 ± 1.6	174.0 ± 0.6	216.0 ± 1.9	243.2 ± 1.2	275.6 ± 3.1

TABLE 6: Adsorption isotherms for united-atom benzene model with TraPPE force field. The number of molecules, N, in a slit amorphous carbon pore as a function of pressure at 298.15 K. Isotherms are based on the adsorption-branch calculations only. The uncertainties were calculated based on 95% confidence intervals

P, Pa	μ, kJ/mol	10 Å	12 Å	14 Å	16 Å	18 Å	20 Å
		Amount adsorbed, N					
1	−71.00	0.0 ± 0.0	0.0 ± 0.0	0.0 ± 0.0	0.0 ± 0.0	0.0 ± 0.0	0.0 ± 0.0
10	−65.30	0.0 ± 0.0	0.0 ± 0.0	0.0 ± 0.0	0.0 ± 0.0	0.0 ± 0.0	0.0 ± 0.0
1×10^2	−59.59	0.1 ± 0.0	0.1 ± 0.0	0.1 ± 0.0	0.1 ± 0.0	0.1 ± 0.0	0.1 ± 0.0
2×10^2	−57.87	0.2 ± 0.0	0.1 ± 0.0	0.1 ± 0.0	0.1 ± 0.0	0.1 ± 0.0	0.1 ± 0.0
4×10^2	−56.15	0.3 ± 0.0	0.2 ± 0.0	0.2 ± 0.0	0.2 ± 0.0	0.2 ± 0.0	0.2 ± 0.0
7×10^2	−54.76	0.6 ± 0.0	0.4 ± 0.0	0.4 ± 0.0	0.4 ± 0.0	0.4 ± 0.0	0.4 ± 0.0
1×10^3	−53.88	0.8 ± 0.0	0.6 ± 0.0	0.6 ± 0.0	0.6 ± 0.0	0.6 ± 0.0	0.6 ± 0.0
2×10^3	−52.16	1.7 ± 0.0	1.3 ± 0.0	1.2 ± 0.0	1.1 ± 0.0	1.1 ± 0.0	1.2 ± 0.0
4×10^3	−50.45	4.7 ± 0.3	2.7 ± 0.1	2.6 ± 0.1	2.4 ± 0.0	2.4 ± 0.0	2.4 ± 0.1
7×10^3	−49.06	140.4 ± 1.9	5.6 ± 0.1	4.9 ± 0.1	4.4 ± 0.1	4.5 ± 0.1	4.5 ± 0.1
1×10^4	−48.18	142.8 ± 1.4	170.3 ± 0.5	7.8 ± 0.2	6.8 ± 0.1	6.7 ± 0.1	6.8 ± 0.2
1×10^5	−47.41	145.6 ± 1.9	172.1 ± 1.7	212.2 ± 1.3	10.3 ± 0.2	10.2 ± 0.4	10.3 ± 0.3
1×10^6	−47.33	146.2 ± 2.3	174.1 ± 2.8	212.1 ± 1.9	10.9 ± 0.1	10.7 ± 0.4	10.8 ± 0.3
1×10^7	−46.55	146.8 ± 1.5	176.4 ± 0.7	215.3 ± 1.8	245.6 ± 1.2	279.9 ± 1.5	17.2 ± 0.7

TABLE 7: Adsorption isotherms for united-atom benzene model with TraPPE force field. The number of molecules, N, in a slit graphitic carbon pore as a function of pressure at 298.15 K. Isotherms are based on the adsorption-branch calculations only. The uncertainties were calculated based on 95% confidence intervals

P, Pa	μ, kJ/mol	10 Å	12 Å	14 Å	16 Å	18 Å	20 Å
		Amount adsorbed, N					
1	−71.00	0.0 ± 0.0	0.0 ± 0.0	0.0 ± 0.0	0.0 ± 0.0	0.0 ± 0.0	0.0 ± 0.0
10	−65.30	87.1 ± 0.6	115.9 ± 1.3	7.8 ± 0.3	4.6 ± 0.2	4.0 ± 0.1	3.9 ± 0.2
1×10^2	−59.59	93.3 ± 1.4	132.5 ± 3.0	150.1 ± 1.2	48.2 ± 1.8	31.6 ± 1.1	29.0 ± 0.8
2×10^2	−57.87	94.3 ± 1.4	132.8 ± 2.1	154.7 ± 1.2	182.5 ± 2.1	61.0 ± 1.2	52.8 ± 1.8
4×10^2	−56.15	97.1 ± 1.3	136.2 ± 1.0	158.8 ± 2.0	191.6 ± 2.1	211.9 ± 0.7	91.0 ± 0.7
7×10^2	−54.76	96.1 ± 2.0	136.5 ± 0.9	161.7 ± 1.9	195.3 ± 1.3	220.1 ± 1.6	114.8 ± 0.4
1×10^3	−53.88	97.0 ± 1.7	142.8 ± 3.2	162.8 ± 1.2	198.7 ± 1.3	223.7 ± 1.5	248.1 ± 1.9
2×10^3	−52.16	98.0 ± 0.5	144.0 ± 0.0	165.0 ± 1.9	203.8 ± 2.4	229.6 ± 2.5	259.1 ± 2.6
4×10^3	−50.45	98.1 ± 1.1	143.6 ± 1.0	167.3 ± 2.7	204.9 ± 2.0	233.7 ± 4.6	264.9 ± 3.8
7×10^3	−49.06	99.3 ± 2.1	144.0 ± 0.1	170.2 ± 4.1	209.1 ± 2.0	236.4 ± 3.7	270.8 ± 1.5
1×10^4	−48.18	99.4 ± 0.9	148.5 ± 3.7	170.6 ± 1.9	216.2 ± 2.7	238.6 ± 3.0	271.3 ± 3.2
1×10^5	−47.41	100.4 ± 1.4	140.0 ± 0.0	172.1 ± 3.8	216.3 ± 1.5	240.4 ± 2.6	275.2 ± 1.1
1×10^6	−47.33	97.2 ± 0.3	144.0 ± 0.0	171.9 ± 2.7	212.6 ± 3.5	240.1 ± 2.5	275.1 ± 2.1
1×10^7	−46.55	101.0 ± 0.0	143.6 ± 1.6	174.7 ± 0.9	212.9 ± 1.9	242.0 ± 2.1	277.4 ± 3.2

First of all, there was a considerable difference in adsorption isotherms for amorphous and graphitic carbon for both benzene models, where both TraPPE and OPLS show the same trend: benzene filled the graphitic slit pore at a lower pressure than the amorphous pore. At high pressures, when the pores are filled, the amount of adsorbed benzene N_0 is different for amorphous and graphitic pores of the same size, but the same for both benzene models.

Analysis of the structure of confined benzene fluid

After equilibration, fluid formed a pronounced layered structure inside the pore regardless of the benzene model. To analyze the layering, we calculated the density profile of benzene inside the slit pore and the orientation of the molecules relative to the carbon walls. The number of molecules used in this MD simulation corresponds to the number of molecules averaged from the three highest pressures in each GCMC run. Firstly, we compared the density distribution $\rho(z)$ for benzene using one force field but different wall structures. The results for the OPLS benzene model in the pores with graphitic and amorphous carbon walls

are presented in Fig. 7a and Fig. 7b, respectively. The zero of the z-axis corresponds to the center of the pore.

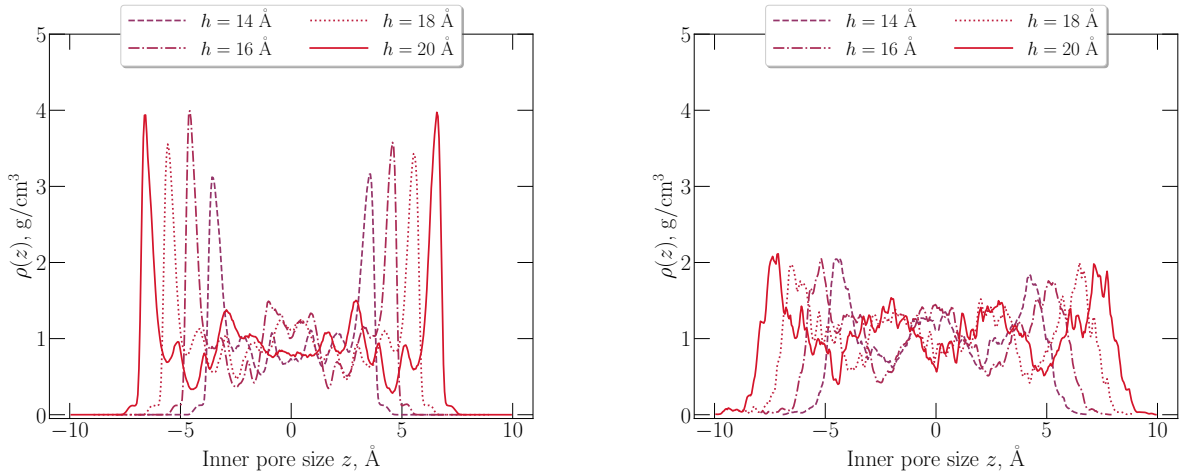

FIGURE 7: Density profiles of all atom OPLS benzene inside carbon slit pore with (a) graphitic and (b) amorphous carbon walls. The results for four different inner sizes of the pore were plotted: 14-20 Å

The peaks of the density profiles correspond to the layers in the pore. The number of peaks for both cases was the same, however, their shapes were different. In the pore with the graphitic walls (Fig. 7a), there was a more distinct layering than in the pore with the amorphous carbon walls (Fig. 7b). Perhaps, this can be explained by the fact that graphite and benzene have a hexagonal structure at the base, so their interaction leads to parallel orientation of the benzene molecules. As it is seen from the simulation snapshots in Fig. 8a and Fig. 8b, for the amorphous wall, the number of benzene molecules, which were perpendicular to the wall surface was higher than with graphitic wall.

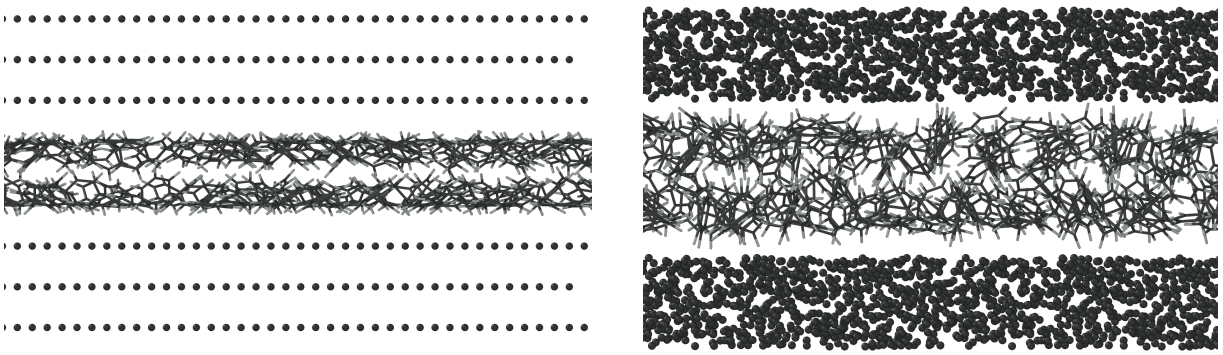

(a) (b)

FIGURE 8: Snapshot of the OPLS all atom benzene and carbon slit pore with with (a) graphitic and (b) amorphous walls. The inner size of the pore is 12 Å.

Also, similarly to Ref. 32, we examined the effect of internal pore size on the layering. There were three benzene layers with graphitic and amorphous carbon for the pore sizes in range from 10 Å to 16 Å. However, an increase in pore size resulted in less structured layers. Eventually, for pore size 20 Å there were two pronounced peaks near the walls and the uniform distribution of benzene molecules between them. This was due to the benzene molecules in the middle of the pore having a weaker interaction with the walls. The same behavior of benzene was observed for the amorphous carbon pore.

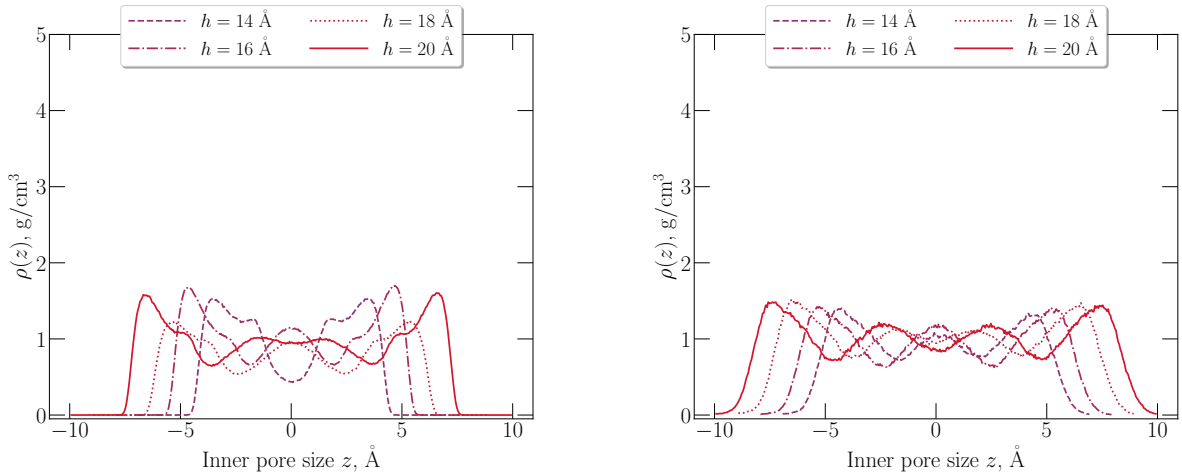

FIGURE 9: Density profiles of 9 site united atom TraPPE benzene inside carbon slit pore with (a) graphitic and (b) amorphous walls. The results for four different inner sizes of the pore were plotted: 14-20 Å

For TraPPE benzene model the density profiles are presented in Fig. 9a and Fig. 9b. We used the same limits on y-axis in Fig. 9, as in Fig. 7 to emphasize the differences in the layering of benzene. There was still a difference between the graphitic and amorphous carbon pore, however, it was not as significant as it was in the case of the OPLS benzene model. The density distribution of benzene in both amorphous and graphitic carbon pores was relatively smooth, which means that the orientation of the molecules inside these pore was also similar. Such preference in the configuration of the benzene molecules leads to the main difference between the TraPPE and OPLS benzene models: for the small pore size, the number of formed layers was different.

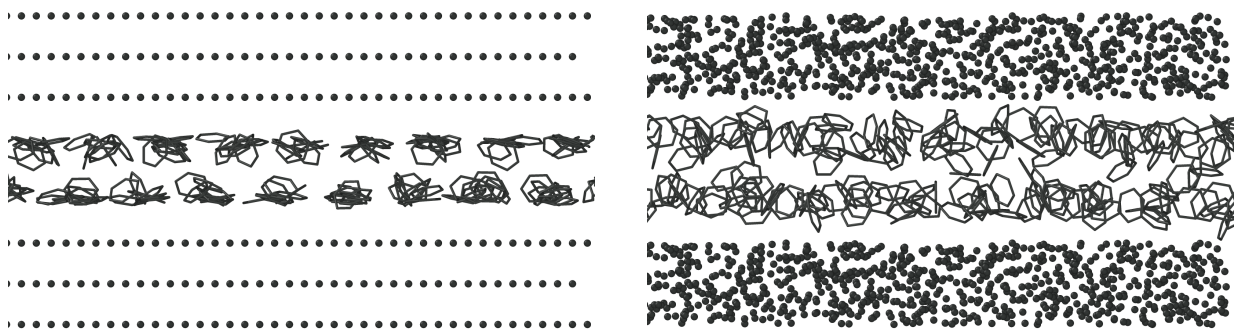

(a) (b)

FIGURE 10: Snapshot of 9 site united atom benzene model and carbon slit pore with (a) graphitic and (b) amorphous walls. The inner size of the pore is 14 Å. Graphitic and amorphous pore were considered for both cases.

Fig. 10a and 10b show the snapshots of the benzene molecules inside 14 Å pores made of graphitic or amorphous carbon. The benzene molecules formed layers, and they preferred the perpendicular orientation to the wall surfaces. The orientation of benzene molecules was quantified using an order parameter based on the second-order Legendre polynomial, which is a common approach in the literature[32,39,76–78]:

$$P_2(z) = \left\langle \frac{1}{2}\left(3\cos^2\theta - 1\right)\right\rangle_z , \tag{1}$$

where the angle θ is the angle between a normal to the benzene ring plane and the z-axis (axis normal to the plane of the walls). Angle brackets is an average over molecules in a layer for considered configurations. The Legendre polynomial defines the orientation of molecules in the pore, e.g. if the molecules are parallel to the pore walls, then $P_2 = 1$. If they are normal to the walls, then $P_2 = -0.5$. Note that some of the works use the first-order Legendre polynomials to quantify the orientation of the molecules.[78–80] However, due to the symmetry of benzene molecules with respect to the mirror plane perpendicular to the z-axis, the first-order polynomials are zero, and are not applicable here for the analysis of the order.

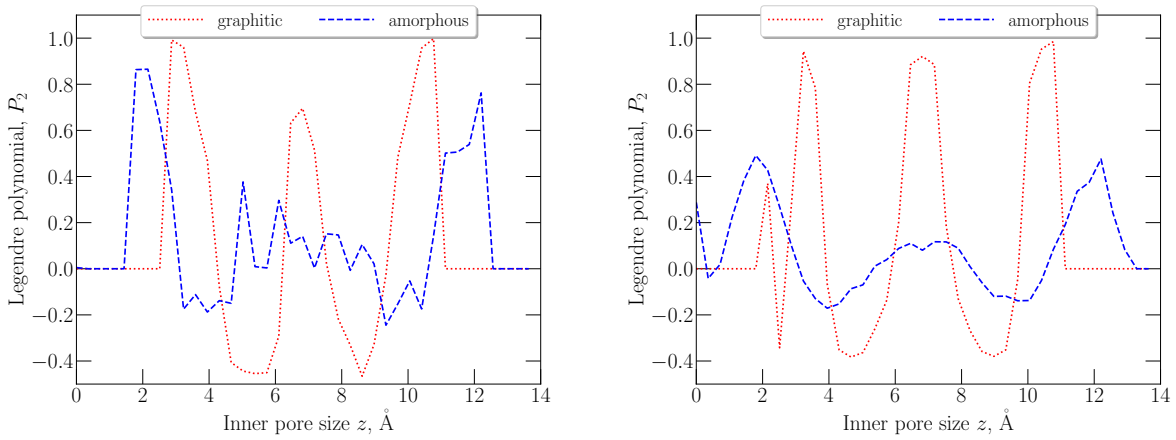

FIGURE 11: Legendre polynomial $P_2(z)$ for the benzene in carbon pores represented by two force fields: (a) all-atom OPLS and (b) 9-site united atom TraPPE

Fig. 11 shows Legendre polynomial calculated for benzene in graphitic and amorphous walls structures. We divided the inner pore size into 40 segments and calculated the average for all of them. Over the simulation time, 250 configurations were used. Although the curves in Fig. 11 are somewhat jagged, they show the layering of the benzene inside the pore. Similar plots were obtained by Fomin in Ref. 32. It should be noted that the Legendre polynomial does not contain any information about the number of molecules with the preferred direction, e.g., if a layer contains only two molecules of the same orientation, the polynomial would give the same value as for a layer with 200 molecules of the same orientation. So based on this function, one can only judge of preferred orientation in a layer of a δz width (δz was defined as the inner size of the pore divided into 50 or 100 segments for OPLS and TraPPE benzene models, respectively). To estimate the percent of molecules perpendicular and parallel to the pore plane we introduced $P_\perp(z)$ and $P_\parallel(z)$:

$$P_\perp(z) = \left\langle \frac{1}{N} \sum P_2(\theta > 45^\circ) \right\rangle \qquad P_\parallel(z) = \left\langle \frac{1}{N} \sum P_2(\theta < 45^\circ) \right\rangle , \tag{2}$$

where N is the number of benzene molecules in a slit pore. $P_\perp(z)$ and $P_\parallel(z)$ presented in

Fig. 12 for 14 Å carbon slit pore supports the conclusion derived from the analysis of density profiles shown in Figs. 7 and 9. The number of layers correlated with the density profiles and the OPLS benzene molecules preferred parallel orientation to the wall surface in graphitic pore more than in the amorphous carbon pore. For the TraPPE model, the fraction of the perpendicular oriented molecules increased in graphitic carbon pore. The percent of perpendicular and parallel molecules in the carbon slit pore for each case is presented in Table 8.

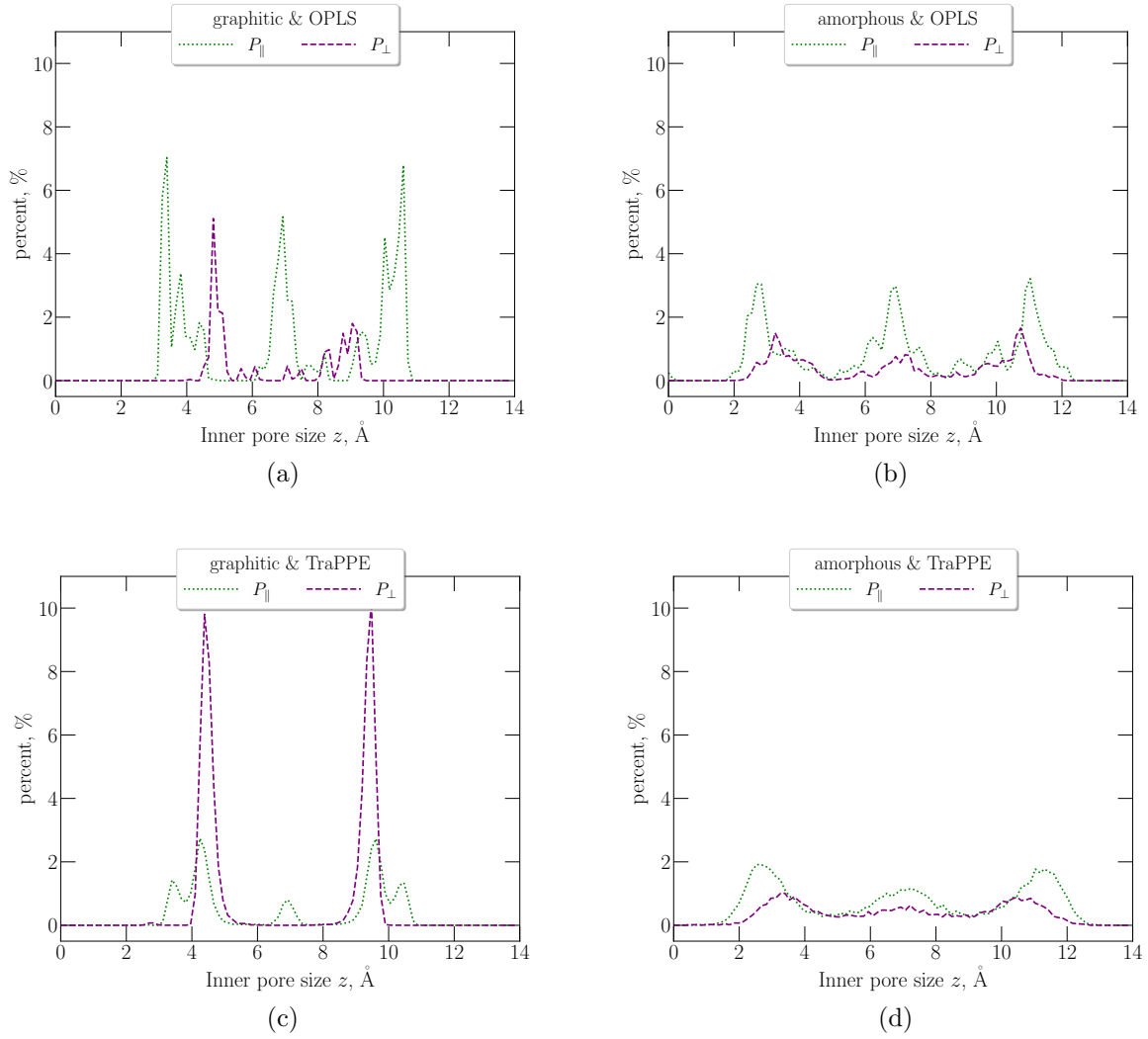

FIGURE 12: Legendre polynomial distribution of benzene in a carbon slit pore: (a) graphitic walls with all atom OPLS benzene model, (b) amorphous walls with all atom OPLS benzene model, (c) graphitic walls with a 9 site united atom TraPPE benzene model and (d) amorphous with a 9 site united atom TraPPE benzene model. $P_\parallel$ and $P_\perp$ show the percent of the benzene molecules in a pore, which are oriented parallel or perpendicular with respect to the pore walls.

Table 8 shows that OPLS benzene molecules preferentially orient parallel to the pore walls irrespective of the different types of the carbon surface. However, from Fig. 12 one can notice that the distribution of the molecules is smoother for amorphous slit pores than for graphitic walls. The preferred orientation of benzene molecules changes if TraPPE force field is used instead of OPLS. For TraPPE, the orientation of molecules in amorphous and graphitic pores become noticeably different (Table 8). This orientation effect can be explained by the

benzene quadrupole moment in the TraPPE model.

TABLE 8: The percent of benzene molecules, oriented perpendicular ($P_\perp$) and parallel ($P_\parallel$) to the pore walls in the carbon slit pore.[a]

	$P_\parallel$	$P_\perp$
Amorphous & OPLS	$70.45 \pm 0.91\%$	$29.55 \pm 0.91\%$
Graphitic & OPLS	$78.19 \pm 0.31\%$	$21.81 \pm 0.31\%$
Amorphous & TraPPE	$64.89 \pm 1.07\%$	$35.11 \pm 1.07\%$
Graphitic & TraPPE	$34.96 \pm 0.47\%$	$65.04 \pm 0.47\%$

[a] The uncertainties were estimated based on block-average method: the simulation is divided into 5 blocks, and the standard deviation is calculated.

Discussion

Adsorption of various combustion products such as polyaromatic hydrocarbons (PAHs) on the surface of atmospheric soot particles plays a significant role in soot evolution. Soot particles include carbon in both graphitic and amorphous forms; therefore, one needs to quantify the interactions of PAHs with both types of carbon surfaces. As a first step towards this goal, in this work we considered the interaction of benzene with two types of carbon surfaces. More specifically, we studied the adsorption of benzene in model slit pores of different sizes using the grand canonical Monte Carlo simulations. Additionally, we studied the structure of liquid-like benzene in the pores by analyzing the configurations obtained from molecular dynamics simulations.

Molecular simulation studies of benzene adsorption have been reported in many papers, and we would like to discuss our results in the context of some of the recent works. We followed the work of Do and Do,[35] who simulated benzene adsorption in *graphitic* slit pores only. Similarly to their work we focused on two different force fields for benzene: all-atom OPLS force field in which all the charges are distributed in a plane,[50] and the united-atom TraPPE force field,[51] in which a benzene molecule was represented with nine sites, three of which were introduced to model the out-of-plane π electron clouds. Despite the distinct

difference between the two benzene models, OPLS and TraPPE, the resulting adsorption isotherms differ insignificantly for the same pore sizes. Our results for graphitic pores, although performed using a different Monte Carlo code, are fully consistent with the results from Ref. 35, and other simulation data.[33] We show that for amorphous pores the adsorption isotherms obtained using two different force fields also do not differ much. As Coasne et al. predicted in their work,[34] the choice of the benzene model did not have a quantitative effect on the adsorption isotherm, unlike on the density distribution. Due to the absence of the experimental data for the system with amorphous walls, previously published simulations[33] compared their results with experimental isotherms measured by Yun et al.[23] for benzene adsorption on activated carbon fibers (ACF). However, due to the wide pore distribution, ACF and amorphous carbon pore are not comparable, even though there is a similarity between ACF structure and modeled amorphous carbon.

The comparison of the adsorption isotherms for the pores of the same size but different surface structure showed, however, a pronounced difference. Filling in an amorphous carbon pore takes place at a pressure of 3-4 orders of magnitude higher than in the graphitic pore of the same size. This difference can be explained by the difference in surface density of the carbon atoms in the walls. In work 81, it was shown that the mere presence of carbon atoms on the surface decreases the density of the fluid layer adjacent to the wall. Thus, the roughness of the atomistic amorphous pore can change simulations results. There are several molecular modeling works that focused on the effect of atomistic roughness of carbon surface on adsorption.[82–86] Long et al.[82] showed that the increase of the wall roughness can drastically decrease the in-pore pressure, which depends on the structure of the adsorbate. During adsorption, fluids would like to fill the cavities in the wall's surface, making the contact layer less structured. For nanoscale slit pores, this surface effect can change all fluid ordering inside a pore, which we observed in our simulations.

In addition to the adsorption isotherms, we studied the microscopic structure of benzene in the pores. We compared the density profiles in the filled pores and observed the expected

difference – more pronounced structuring in the pores with the graphitic walls compared to the pores with amorphous walls. This difference is observed in both force fields. Further analysis was performed based on the Legendre polynomials, which characterize the spatial orientation of the benzene rings. Our results using the OPLS force field are in line with the data reported earlier by Coasne et al.[34] for graphitic pores and by Fomin[32] for both graphitic and amorphous pores. However, the second-order Legendre polynomials obtained from the TraPPE united-atom force field appeared noticeably different. Table 8 shows that for TraPPE benzene molecules, the preference in orientation is perpendicular to the wall surface. This difference, pointed out earlier by Do and Do[35] for graphitic pore, is due to the non-zero quadrupole moment of benzene molecules in TraPPE force field. To our knowledge, for the amorphous pores, we are reporting this effect for the first time. Table 9 gives the quadrupole moments of benzene molecules calculated for both representations using RASPA software. Only diagonal elements of the quadrupole tensor are essential for potential fields generated by an electrically neutral system such as benzene. Comparison to the literature shows that while the quadrupole moment from the TraPPE model is reasonably close to experimental values, the OPLS model gives nearly a zero moment.

The chosen OPLS and TraPPE force fields are readily available in standard molecular simulation codes. However, other force fields, parameterized with quadrupole moments in mind, could provide more rigorous results. One of such candidates is the electrostatic version of the Anisotropic United Atom (AUA) force field for benzene.[87] While AUA has been extended to other chemicals,[88–90] including PAHs,[91] the use of this force field is limited, because it is not implemented in codes in this work.

TABLE 9: Diagonal elements Q_{xx}, Q_{yy}, and Q_{zz} of the quadrupole moment tensor for the OPLS (all atom)[50] and TraPPE (united atom)[51] models of benzene

	Q_{xx}, D Å	Q_{yy}, D Å	Q_{zz}, D Å
OPLS	0.036	0.036	−0.072
TraPPE	3.47	3.47	−6.96
Experiment[92]	2.8	2.8	−5.6
Num. Calc.[93]	3.3	3.3	−6.6

Our work was motivated by the interest in the soot restructuring process in which solvation forces in the adsorbed liquid films play a key role.[7,94] These forces depend on the solid-fluid interactions, the fluid structure, and the solid surface structure.[95–97] The difference in microstructure of adsorbed benzene in graphitic and amorphous pores is likely to affect these forces significantly. Furthermore, although our study predicts very close adsorption isotherms for two different force fields, the observed dependence of microstructure on the choice of the force field suggests that the solvation forces can be substantially different depending on the force field used. These calculations, however, are a subject of a separate study.

Conclusion

Motivated by the problem of condensation-induced restructuring of atmospheric soot, we studied the interaction between benzene molecules (as the simplest example of a chemical substance with an aromatic ring) and slit carbon pore with different structures of the pore walls. To estimate the role of the quadrupole moment, we used two different force fields for benzene (all-atom and united atom). The results showed that the choice of the benzene model did not affect the adsorption isotherms. However, the quadrupole moment significantly changed the liquid distribution inside the pore. In addition, the choice of model used to represent the carbon surface (graphitic or amorphous walls) significantly affects the simulated adsorption process. Overall, our work contributes to providing molecular simulation adsorption data, which is specifically of interest for environmental applications.

Acknowledgments

This work was supported by the National Science Foundation. E.V.I., A.F.K., and G.Y.G. were supported by CBET-2128679, A.E. was supported by CBET-1944495. We would like to thank Ali Hasani for providing a TEM micrograph of soot particles, and Benoit Coasne

and Javier Perez-Pellitero for stimulating discussions.

Supporting Information

The Supporting Information is available free of charge on the ACS Publications website at DOI: 10.1021/acs.jced.2c00063

Selected input files for Monte Carlo and molecular dynamics simulations. Simulation input files of generation of the amorphous structure for the carbon slit pore. Adsorption data in AIF format.

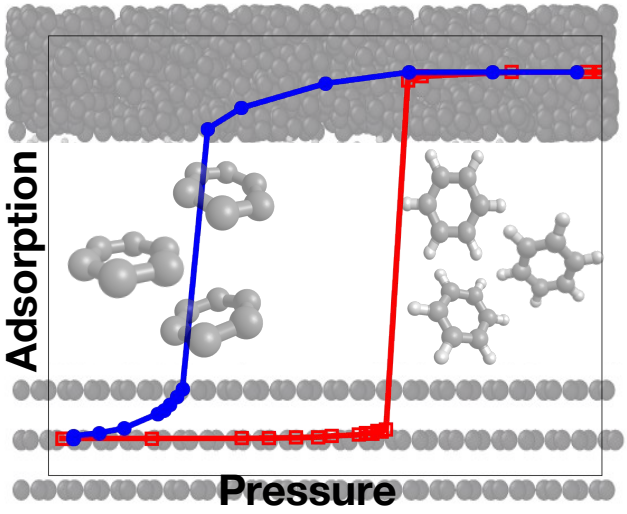

FIGURE 13: TOC graphics

References

(1) Bond, T. C.; Doherty, S. J.; Fahey, D.; Forster, P.; Berntsen, T.; DeAngelo, B. J.; Flanner, M. G.; Ghan, S.; Kärcher, B.; Koch, D., et al. Bounding the role of black carbon in the climate system: A scientific assessment. *J. Geophys. Res. Atmos.* **2013**, *118*, 5380–5552.

(2) Shiraiwa, M.; Selzle, K.; Pöschl, U. Hazardous components and health effects of atmospheric aerosol particles: reactive oxygen species, soot, polycyclic aromatic compounds and allergenic proteins. *Free Radical Res.* **2012**, *46*, 927–939.

(3) Faccinetto, A.; Desgroux, P.; Ziskind, M.; Therssen, E.; Focsa, C. High-sensitivity detection of polycyclic aromatic hydrocarbons adsorbed onto soot particles using laser desorption/laser ionization/time-of-flight mass spectrometry: An approach to studying the soot inception process in low-pressure flames. *Combust. Flame* **2011**, *158*, 227–239.

(4) Kim, K.-H.; Jahan, S. A.; Kabir, E.; Brown, R. J. A review of airborne polycyclic aromatic hydrocarbons (PAHs) and their human health effects. *Environ. Int.* **2013**, *60*, 71–80.

(5) Chen, C.; Fan, X.; Shaltout, T.; Qiu, C.; Ma, Y.; Goldman, A.; Khalizov, A. F. An unexpected restructuring of combustion soot aggregates by subnanometer coatings of polycyclic aromatic hydrocarbons. *Geophys. Res. Lett.* **2016**, *43*, 1–9.

(6) Hinds, W. C. *Aerosol technology: properties, behavior, and measurement of airborne particles*; John Wiley & Sons, 1999.

(7) Chen, C.; Enekwizu, O. Y.; Fan, X.; Dobrzanski, C. D.; Ivanova, E. V.; Ma, Y.; Gor, G. Y.; Khalizov, A. F. Single Parameter for Predicting the Morphology of Atmospheric Black Carbon. *Environ. Sci. Technol.* **2018**, *52*, 14169–14179.

(8) Ivanova, E. V.; Khalizov, A. F.; Gor, G. Y. Kinetic model for competitive condensation of vapor between concave and convex surfaces in a soot aggregate. *Aerosol Sci. Technol.* **2020**, *55*, 302–315.

(9) Slowik, J. G.; Cross, E. S.; Han, J.-H.; Kolucki, J.; Davidovits, P.; Williams, L. R.; Onasch, T. B.; Jayne, J. T.; Kolb, C. E.; Worsnop, D. R. Measurements of morphology changes of fractal soot particles using coating and denuding experiments: Implications for optical absorption and atmospheric lifetime. *Aerosol Sci. Technol.* **2007**, *41*, 734–750.

(10) Weingartner, E.; Baltensperger, U.; Burtscher, H. Growth and structural change of combustion aerosols at high relative humidity. *Environ. Sci. Technol.* **1995**, *29*, 2982–2986.

(11) Miljevic, B.; Surawski, N. C.; Bostrom, T.; Ristovski, Z. D. Restructuring of carbonaceous particles upon exposure to organic and water vapours. *J. Aerosol Sci.* **2012**, *47*, 48–57.

(12) Kütz, S.; Schmidt-Ott, A. Characterization of agglomerates by condensation-induced restructuring. *J. Aerosol Sci.* **1992**, *23*, 357–360.

(13) Mikhailov, E. F.; Vlasenko, S. S.; Krämer, L.; Niessner, R. Interaction of soot aerosol particles with water droplets: influence of surface hydrophilicity. *J. Aerosol Sci.* **2001**, *32*, 697–711.

(14) Schnitzler, E. G.; Dutt, A.; Charbonneau, A. M.; Olfert, J. S.; Jäger, W. Soot aggregate restructuring due to coatings of secondary organic aerosol derived from aromatic precursors. *Environ. Sci. Technol.* **2014**, *48*, 14309–14316.

(15) Botero, M. L.; Sheng, Y.; Akroyd, J.; Martin, J.; Dreyer, J. A.; Yang, W.; Kraft, M. Internal structure of soot particles in a diffusion flame. *Carbon* **2019**, *141*, 635–642.

(16) Davis, J.; Molnar, E.; Novosselov, I. Nanostructure transition of young soot aggregates to mature soot aggregates in diluted diffusion flames. *Carbon* **2020**, *159*, 255–265.

(17) Michelsen, H. A.; Colket, M. B.; Bengtsson, P.-E.; D'anna, A.; Desgroux, P.; Haynes, B. S.; Miller, J. H.; Nathan, G. J.; Pitsch, H.; Wang, H. A review of terminology used to describe soot formation and evolution under combustion and pyrolytic conditions. *ACS Nano* **2020**, *14*, 12470–12490.

(18) Fernández, C. G.; Picaud, S.; Devel, M. Calculations of the mass absorption cross sections for carbonaceous nanoparticles modeling soot. *J. Quant. Spectrosc. Radiat. Transfer* **2015**, *164*, 69–81.

(19) Isirikyan, A.; Kiselev, A. The absolute adsorption isotherms of vapors of nitrogen, benzene and n-hexane, and the heats of adsorption of benzene and n-hexane on graphitized carbon blacks. I. Graphitized thermal blacks. *J. Phys. Chem.* **1961**, *65*, 601–607.

(20) Pierotti, R.; Smallwood, R. The adsorption of benzene on homogeneous substrates. *J. Colloid Interface Sci.* **1966**, *22*, 469–481.

(21) Pierce, C.; Ewing, B. Localized adsorption on graphite surfaces. *J. Phys. Chem.* **1967**, *71*, 3408–3413.

(22) Yun, J.-H.; Choi, D.-K. Adsorption isotherms of benzene and methylbenzene vapors on activated carbon. *Journal of Chemical & Engineering Data* **1997**, *42*, 894–896.

(23) Yun, J.-H.; Hwang, K.-Y.; Choi, D.-K. Adsorption of benzene and toluene vapors on activated carbon fiber at 298, 323, and 348 K. *Journal of Chemical & Engineering Data* **1998**, *43*, 843–845.

(24) Meehan, P.; Rayment, T.; Thomas, R. K.; Bomchil, G.; White, J. W. Neutron diffraction from benzene adsorbed on graphite. *J. Chem. Soc., Faraday Trans. 1 F* **1980**, *76*, 2011–2016.

(25) Vernov, A.; Steele, W. A. Computer simulations of benzene adsorbed on graphite. 1. 85 K. *Langmuir* **1991**, *7*, 3110–3117.

(26) Vernov, A.; Steele, W. A. Computer simulations of benzene adsorbed on graphite. 2. 298 k. *Langmuir* **1991**, *7*, 2817–2820.

(27) Matties, M. A.; Hentschke, R. Molecular dynamics simulation of benzene on graphite. 2. Phase behavior of adsorbed multilayers. *Langmuir* **1996**, *12*, 2501–2504.

(28) Matties, M. A.; Hentschke, R. Molecular dynamics simulation of benzene on graphite: 1. Phase behavior of an adsorbed monolayer. *Langmuir* **1996**, *12*, 2495–2500.

(29) Clifton, B.; Cosgrove, T. Simulation of liquid benzene between two graphite surfaces: a molecular dynamics study. *Mol. Phys.* **1998**, *93*, 767–776.

(30) Klomkliang, N.; Do, D.; Nicholson, D. Affinity and packing of benzene, toluene, and p-xylene adsorption on a graphitic surface and in pores. *Ind. Eng. Chem. Res.* **2012**, *51*, 5320–5329.

(31) Klomkliang, N.; Do, D.; Nicholson, D.; Tangsathitkulchai, C.; Wongkoblap, A. Multilayer adsorption of benzene on graphitised thermal carbon black—The importance of quadrupole and explicit hydrogen in the potential model. *Chem. Eng. Sci.* **2012**, *69*, 472–482.

(32) Fomin, Y. D. Molecular dynamics simulation of benzene in graphite and amorphous carbon slit pores. *J. Comput. Chem* **2013**, *34*, 2615–2624.

(33) Diao, R.; Zhang, H.; Zhao, D.; Li, S. Adsorption and structure of benzene, toluene, and p-xylene in carbon slit pores: A Monte Carlo simulation study. *Chem. Eng. Sci.* **2019**, *197*, 120–134.

(34) Coasne, B.; Alba-Simionesco, C.; Audonnet, F.; Dosseh, G.; Gubbins, K. E. Adsorption,

structure and dynamics of benzene in ordered and disordered porous carbons. *Phys. Chem. Chem. Phys.* **2011**, *13*, 3748–3757.

(35) Do, D.; Do, H. Adsorption of benzene on graphitized thermal carbon black: Reduction of the quadrupole moment in the adsorbed phase. *Langmuir* **2006**, *22*, 1121–1128.

(36) Hunter, C. A.; Sanders, J. K. The nature of π-π interactions. *J. Am. Chem. Soc.* **1990**, *112*, 5525–5534.

(37) Coasne, B.; Alba-Simionesco, C.; Audonnet, F.; Dosseh, G.; Gubbins, K. E. Molecular simulation of the adsorption and structure of benzene confined in mesoporous silicas. *Adsorption* **2007**, *13*, 485–490.

(38) Coasne, B.; Alba-Simionesco, C.; Audonnet, F.; Dosseh, G.; Gubbins, K. E. Adsorption and structure of benzene on silica surfaces and in nanopores. *Langmuir* **2009**, *25*, 10648–10659.

(39) Coasne, B.; Fourkas, J. T. Structure and dynamics of benzene confined in silica nanopores. *J. Phys. Chem. C* **2011**, *115*, 15471–15479.

(40) Franklin, R. E. The structure of graphitic carbons. *Acta Crystallogr.* **1951**, *4*, 253–261.

(41) Chung, D. Review graphite. *J. Mater. Sci.* **2002**, *37*, 1475–1489.

(42) Beeman, D.; Silverman, J.; Lynds, R.; Anderson, M. Modeling studies of amorphous carbon. *Phys. Rev. B* **1984**, *30*, 870.

(43) Kaukonen, M.; Nieminen, R. M. Atomic-scale modeling of the ion-beam-induced growth of amorphous carbon. *Phys. Rev. B* **2000**, *61*, 2806.

(44) Jäger, H.; Albe, K. Molecular-dynamics simulations of steady-state growth of ion-deposited tetrahedral amorphous carbon films. *J. Appl. Phys* **2000**, *88*, 1129–1135.

(45) Lawson, J. W.; Srivastava, D. Formation and structure of amorphous carbon char from polymer materials. *Phys. Rev. B* **2008**, *77*, 144209.

(46) Harris, P. J. Fullerene-like models for microporous carbon. *J. Mater Sci* **2013**, *48*, 565–577.

(47) Nguyen, T. X.; Cohaut, N.; Bae, J.-S.; Bhatia, S. K. New method for atomistic modeling of the microstructure of activated carbons using hybrid reverse Monte Carlo simulation. *Langmuir* **2008**, *24*, 7912–7922.

(48) Palmer, J. C.; Gubbins, K. E. Atomistic models for disordered nanoporous carbons using reactive force fields. *Micropor. Mesopor. Mat.* **2012**, *154*, 24–37.

(49) Ranganathan, R.; Rokkam, S.; Desai, T.; Keblinski, P. Generation of amorphous carbon models using liquid quench method: A reactive molecular dynamics study. *Carbon* **2017**, *113*, 87–99.

(50) Jorgensen, W. L.; Severance, D. L. Aromatic-aromatic interactions: free energy profiles for the benzene dimer in water, chloroform, and liquid benzene. *J. Am. Chem. Soc.* **1990**, *112*, 4768–4774.

(51) Wick, C. D.; Siepmann, J. I.; Klotz, W. L.; Schure, M. R. Temperature effects on the retention of n-alkanes and arenes in helium–squalane gas–liquid chromatography: experiment and molecular simulation. *J. Chromatogr. A* **2002**, *954*, 181–190.

(52) Wick, C. D.; Martin, M. G.; Siepmann, J. I. Transferable potentials for phase equilibria. 4. United-atom description of linear and branched alkenes and alkylbenzenes. *J. Phys. Chem. B* **2000**, *104*, 8008–8016.

(53) Dubbeldam, D.; Calero, S.; Ellis, D. E.; Snurr, R. Q. RASPA: molecular simulation software for adsorption and diffusion in flexible nanoporous materials. *Mol. Simul.* **2016**, *42*, 81–101.

(54) Liu, A.; Peng, X.; Jin, Q.; Jain, S. K.; Vicent-Luna, J. M.; Calero, S.; Zhao, D. Adsorption and diffusion of benzene in Mg-MOF-74 with open metal sites. *ACS Appl. Mater. Interfaces* **2019**, *11*, 4686–4700.

(55) Wu, Y.; Chen, H.; Liu, D.; Xiao, J.; Qian, Y.; Xi, H. Effective ligand functionalization of zirconium-based metal–organic frameworks for the adsorption and separation of benzene and toluene: a multiscale computational study. *ACS Appl. Mater. Interfaces* **2015**, *7*, 5775–5787.

(56) Tersoff, J. New empirical model for the structural properties of silicon. *Phys. Rev. Lett.* **1986**, *56*, 632.

(57) Marks, N. Modelling diamond-like carbon with the environment-dependent interaction potential. *J. Phys.: Condens. Matter* **2002**, *14*, 2901.

(58) Marks, N. A. Generalizing the environment-dependent interaction potential for carbon. *Phys. Rev. B* **2000**, *63*, 035401.

(59) Suarez-Martinez, I.; Marks, N. Effect of microstructure on the thermal conductivity of disordered carbon. *Appl. Phys. Lett.* **2011**, *99*, 033101.

(60) Shi, Y. A mimetic porous carbon model by quench molecular dynamics simulation. *J. Chem. Phys.* **2008**, *128*, 234707.

(61) Makeev, M. A.; Srivastava, D. Thermal properties of char obtained by pyrolysis: A molecular dynamics simulation study. *Appl. Phys. Lett.* **2009**, *95*, 181908.

(62) Li, L.; Xu, M.; Song, W.; Ovcharenko, A.; Zhang, G.; Jia, D. The effect of empirical potential functions on modeling of amorphous carbon using molecular dynamics method. *Appl. Surf. Sci.* **2013**, *286*, 287–297.

(63) Frenkel, D.; Smit, B.; Ratner, M. A. *Understanding molecular simulation: from algorithms to applications*; Academic press San Diego, 1996; Vol. 2.

(64) Peng, D.-Y.; Robinson, D. B. A new two-constant equation of state. *Industrial & Engineering Chemistry Fundamentals* **1976**, *15*, 59–64.

(65) Verlet, L. Computer "experiments" on classical fluids. I. Thermodynamical properties of Lennard-Jones molecules. *Phys. Rev.* **1967**, *159*, 98.

(66) Humphrey, W.; Dalke, A.; Schulten, K. VMD: visual molecular dynamics. *J. Mol. Graphics* **1996**, *14*, 33–38.

(67) Martínez, L.; Andrade, R.; Birgin, E. G.; Martínez, J. M. PACKMOL: a package for building initial configurations for molecular dynamics simulations. *J. Comput. Chem* **2009**, *30*, 2157–2164.

(68) Jewett, A. I.; Zhuang, Z.; Shea, J.-E. Moltemplate a coarse-grained model assembly tool. *Biophys. J.* **2013**, *104*, 169a.

(69) Jewett, A. I.; Stelter, D.; Lambert, J.; Saladi, S. M.; Roscioni, O. M.; Ricci, M.; Autin, L.; Maritan, M.; Bashusqeh, S. M.; Keyes, T., et al. Moltemplate: A Tool for Coarse-Grained Modeling of Complex Biological Matter and Soft Condensed Matter Physics. *J. Mol. Biol.* **2021**, *433*, 166841.

(70) Plimpton, S. Fast parallel algorithms for short-range molecular dynamics. *J. Comput. Phys.* **1995**, *117*, 1–19.

(71) Dubinin, M. M.; Zhukovskaia, E. G. Adsorption properties of carbon adsorbents Communication 2. Adsorption properties of active carbons with respect to benzene and nitrogen vapors. *Bulletin of the Academy of Sciences of the USSR, Division of chemical science* **1958**, *7*, 519–528.

(72) Kadlec, O.; Dubinin, M. M. Comments on the limits of applicability of the mechanism of capillary condensation. *J. Colloid Interface Sci.* **1969**, *31*, 479–489.

(73) Trznadel, B.; Światkowski, A. On the pore size distributions and fractal dimensions of activated carbons evaluated on the basis of the analysis of nitrogen, argon and benzene vapour adsorption data. *Adsorption Science & Technology* **1999**, *17*, 303–318.

(74) Ramos, M. E.; Bonelli, P. R.; Cukierman, A. L.; Carrott, M. R.; Carrott, P. Adsorption of volatile organic compounds onto activated carbon cloths derived from a novel regenerated cellulosic precursor. *J. Hazard. Mater.* **2010**, *177*, 175–182.

(75) Thommes, M.; Kaneko, K.; Neimark, A. V.; Olivier, J. P.; Rodriguez-Reinoso, F.; Rouquerol, J.; Sing, K. S. Physisorption of gases, with special reference to the evaluation of surface area and pore size distribution (IUPAC Technical Report). *Pure Appl. Chem.* **2015**, *87*, 1051–1069.

(76) Inomata, H.; Saito, S.; Debenedetti, P. G. Molecular dynamics simulation of infinitely dilute solutions of benzene in supercritical CO_2. *Fluid Phase Equilib.* **1996**, *116*, 282–288.

(77) Liu, Y.; Wu, G.; Hu, R.; Gao, G. Effects of aromatics on ionic liquids for C4 alkylation reaction: Insights from scale-up experiment and molecular dynamics simulation. *Chem. Eng. J.* **2020**, *402*, 126252.

(78) Lafrance, C.-P.; Nabet, A.; Prud'homme, R. E.; Pézolet, M. On the relationship between the order parameter and the shape of orientation distributions. *Can. J. Chem.* **1995**, *73*, 1497–1505.

(79) Malani, A.; Ayappa, K.; Murad, S. Influence of hydrophilic surface specificity on the structural properties of confined water. *J. Phys. Chem. B* **2009**, *113*, 13825–13839.

(80) Debbarma, R.; Malani, A. Comparative study of water adsorption on a H+ and K+ ion exposed mica surface: Monte carlo simulation study. *Langmuir* **2016**, *32*, 1034–1046.

(81) Ayappa, K.; Mishra, R. K. Freezing of fluids confined between mica surfaces. *J. Phys. Chem. B* **2007**, *111*, 14299–14310.

(82) Long, Y.; Palmer, J. C.; Coasne, B.; Śliwinska-Bartkowiak, M.; Jackson, G.; Müller, E. A.; Gubbins, K. E. On the molecular origin of high-pressure effects in nanoconfinement: The role of surface chemistry and roughness. *J. Chem. Phys.* **2013**, *139*, 144701.

(83) Neimark, A. V.; Lin, Y.; Ravikovitch, P. I.; Thommes, M. Quenched solid density functional theory and pore size analysis of micro-mesoporous carbons. *Carbon* **2009**, *47*, 1617–1628.

(84) Bakaev, V. Rumpled graphite basal plane as a model heterogeneous carbon surface. *J. Chem. Phys.* **1995**, *102*, 1398–1404.

(85) Turner, A. R.; Quirke, N. A grand canonical Monte Carlo study of adsorption on graphitic surfaces with defects. *Carbon* **1998**, *36*, 1439–1446.

(86) Do, D.; Do, H. Modeling of adsorption on nongraphitized carbon surface: GCMC simulation studies and comparison with experimental data. *J. Phys. Chem. B* **2006**, *110*, 17531–17538.

(87) Nieto-Draghi, C.; Bonet Àvalos, J.; Contreras, O.; Ungerer, P.; Ridard, J. Dynamical and structural properties of benzene in supercritical water. *J. Chem. Phys.* **2004**, *121*, 10566–10576.

(88) Nieto-Draghi, C.; Bonnaud, P.; Ungerer, P. Anisotropic united atom model including the electrostatic interactions of methylbenzenes. II. Transport properties. *J. Phys. Chem. C* **2007**, *111*, 15942–15951.

(89) Contreras-Camacho, R. O.; Ungerer, P.; Ahunbay, M. G.; Lachet, V.; Perez-Pellitero, J.; Mackie, A. D. Optimized intermolecular potential for aromatic hydrocarbons based on

anisotropic united atoms. 2. Alkylbenzenes and styrene. *J. Phys. Chem. B* **2004**, *108*, 14115–14123.

(90) Ahunbay, M. G.; Perez-Pellitero, J.; Contreras-Camacho, R. O.; Teuler, J.-M.; Ungerer, P.; Mackie, A. D.; Lachet, V. Optimized intermolecular potential for aromatic hydrocarbons based on anisotropic united atoms. III. Polyaromatic and naphthenoaromatic hydrocarbons. *J. Phys. Chem. B* **2005**, *109*, 2970–2976.

(91) Creton, B.; de Bruin, T.; Lachet, V.; Nieto-Draghi, C. Extension of a charged anisotropic united atoms model to polycyclic aromatic compounds. *J. Phys. Chem. B* **2010**, *114*, 6522–6530.

(92) Shoemaker, R.; Flygare, W. Molecular Quadrupole Moment, Molecular Magnetic Susceptibilities, and Molecular g Values in Benzene. *J. Chem. Phys.* **1969**, *51*, 2988–2991.

(93) Gierke, T.; Tigelaar, H.; Flygare, W. Calculation of molecular electric dipole and quadrupole moments. *J. Am. Chem. Soc.* **1972**, *94*, 330–338.

(94) Gor, G. Y.; Huber, P.; Bernstein, N. Adsorption-Induced Deformation of Nanoporous Materials - a Review. *Appl. Phys. Rev.* **2017**, *4*.

(95) Israelachvili, J. Solvation forces and liquid structure, as probed by direct force measurements. *Acc. Chem. Res.* **1987**, *20*, 415–421.

(96) Frink, L. J. D.; van Swol, F. Solvation forces between rough surfaces. *J. Chem. Phys.* **1998**, *108*, 5588–5598.

(97) Kolesnikov, A. L.; Budkov, Y. A.; Gor, G. Y. Adsorption-induced deformation of mesoporous materials with corrugated cylindrical pores. *J. Chem. Phys.* **2020**, *153*, 194703.